*energies*

MDPI

*Article*

# Comparative Thermodynamic Analysis of the Performance of an Organic Rankine Cycle Using Different Working Fluids

**Ladislao Eduardo Méndez-Cruz [1], Miguel Ángel Gutiérrez-Limón [2], Helen Lugo-Méndez [1], Raúl Lugo-Leyte [3], Teresa Lopez-Arenas [1] and Mauricio Sales-Cruz [1,*]**

[1] Departamento de Procesos y Tecnología, Universidad Autónoma Metropolitana—Cuajimalpa, Av. Vasco de Quiroga No. 4871, Colonia Santa Fé, Cuajimalpa 05348, Mexico; 2201801516@cua.uam.mx (L.E.M.-C.); hlugo@cua.uam.mx (H.L.-M.); mtlopez@cua.uam.mx (T.L.-A.)
[2] Departamento de Energía, Universidad Autónoma Metropolitana—Azcapotzalco, Av. San Pablo No. 180, Colonia Reynosa Tamaulipas, Azcapotzalco 02200, Mexico; magl@azc.uam.mx
[3] Departamento de Ingeniería de Procesos e Hidráulica, Universidad Autónoma Metropolitana—Iztapalapa, Av. Ferrocarril San Rafael Atlixco No. 186, Colonia Leyes de Reforma 1A Sección, Iztapalapa 09310, Mexico; lulr@xanum.uam.mx
* Correspondence: asales@cua.uam.mx

**Abstract:** Today, the study of thermal systems that take advantage of residual thermal sources in the power generation sector is of great importance to mitigate environmental impact and promote sustainable alternatives in this sector. Among these alternatives, the organic Rankine cycle (ORC) is of great relevance since it allows taking advantage of residual energy sources at low temperatures. This work presents a methodology to evaluate the feasibility of using a refrigerant as a working fluid in an organic Rankine cycle based on an exergetic viability index. As a case study, R134a, R600a, R245fa, and R123 refrigerants were considered. A residual thermal source was used that came from the Hybrid Cycle Plant of the Valley of Mexico. Thermodynamic analysis was performed to determine generated power, thermal efficiency, refrigerant mass flow, pinch point temperature difference, specific steam consumption, unused thermal exergy flow, exergy efficiency, and total heat transfer requirement. The weighted average of the differences between these indicators, the global warming index, and the ozone depletion potential relative to the most favorable indicator corresponded to the definition of the exergetic viability index of the refrigerant. The results indicate that the ORC operating at condensing temperatures of 25, 35, and 45 °C with R245fa shows the highest rate of exergetic viability despite not generating the greatest amount of power and being one of the refrigerants with the highest total heat transfer requirement. Finally, at condensing temperatures above 45 °C, it is observed that R600a is exergetically the most viable refrigerant used in the ORC.

**Keywords:** working fluid selection; exergetic efficiency; organic Rankine cycle; waste heat



**Citation:** Méndez-Cruz, L.E.; Gutiérrez-Limón, M.Á.; Lugo-Méndez, H.; Lugo-Leyte, R.; Lopez-Arenas, T.; Sales-Cruz, M. Comparative Thermodynamic Analysis of the Performance of an Organic Rankine Cycle Using Different Working Fluids. *Energies* **2022**, *15*, 2588. https://doi.org/10.3390/en15072588

Received: 4 February 2022
Accepted: 30 March 2022
Published: 1 April 2022



## 1. Introduction

In recent years, industrialization, population growth, and a trend towards a better quality of life have led to an increase in the demand for fossil fuels and a deterioration of the environment. Currently there is a transition towards the use of renewable energies, but these are not yet entirely viable. Therefore, it is imperative to adopt and develop alternative forms for power generation that take advantage, on the one hand, of residual thermal energy from current power generation technologies [1] and, on the other hand, of primary thermal energy from geothermal and solar energy [2]. Organic Rankine cycles (ORCs) have been presented as a possible alternative that uses low-temperature streams of matter to generate powers from 10 kW to 10 MW. ORCs are characterized by their adaptability to recover energy from any thermal source in combination with an organic fluid that favors cycle performance [3]. Among the residual thermal sources are the combustion gases produced in conventional thermal power plants discharged into the environment at

temperatures ranging between 400 °C and 150 °C and between 320 °C and 60 °C for the burning of fossil fuels and biomass, respectively. These streams represent 52% of residual thermal energy dissipated to the environment without being used [4]. Within renewable thermal sources are the geothermal resources available at temperatures of 350 °C to 100 °C and the oil streams heated to temperatures of 500 °C to 80 °C in parabolic and flat-plate collectors [5,6].

There are a large number of organic working fluids used in ORCs, such as R134a, R600a, R245fa, R123, $NH_3$, R123, and R142b, among others. Fluid selection depends on the joint analysis of various criteria in the ORC performance: safety of use, impact on the environment, energy and exergy criteria, and economic aspects, among others. These criteria are based on different indicators, such as the thermodynamic behavior of the fluid with the conditions of the thermal source in the liquid–vapor equilibrium; the performance of the cycle as a function of the thermal efficiency parameters (work output, generated power and the pinch point temperature difference in the evaporator), exergetic efficiency, exergy ratio of the residues, and sustainability index; and some indicators of environmental impact and human toxicity of organic fluids [3,4,7–11].

In the literature, there are various energy analyses that have evaluated ORC performance with different organic fluids. Kajurek et al. [12] determined the maximum efficiencies of a conventional ORC for R245fa and $NH_3$ and the maximum power for R134a and R123 within a set of ten working fluids. It was also shown that maximum energy generation is a function of the temperature of the thermal source and the properties of the organic fluid, resulting in an optimal source temperature range for R134a and R123 from 100 °C to 180 °C, while the range for R245fa was between 185 °C and 210 °C. Raghulnath et al. [13] evaluated the performance of an ORC whose thermal source was the energy contained in the combustion gases of an internal combustion engine at temperatures from 120 to 280 °C. Five different refrigerants were compared, and it was reported that the maximum generated powers of 8.21 and 6.27 kW were obtained using R600a and R11 as working fluids, respectively. Abdalla et al. [14] evaluated an ORC with a heat exchanger for eight different organic fluids and found that R245fa was the fluid with the maximum power and thermal efficiency at 39.96 kW and 15.1%, respectively. Vélez et al. [15] analyzed an ORC with a heat exchanger using R134a and reported that the thermal efficiency of the cycle increased with the relationship between inlet pressure to the turbine and condensation when the temperature of the thermal source was kept constant at 150 ° C. Wang et al. [16] maximized the power generation and thermal efficiency of an ORC using a 150 °C heat source and R123, R245fa, and R600a as working fluids. Their optimization model showed that the maximum generated power and thermal efficiency was obtained with R600a, considering as decision variables turbine inlet pressure and temperature, pinch point temperature difference, and steam generator transfer areas and condenser. Bamorovat et al. [17] experimentally evaluated an ORC with R245fa and a mixture of 60% R245fa and 40% R134a, varying the temperature of the heat source from 80 to 120 °C. They found out that this mixture led to higher power compared to pure R245fa refrigerant. Surindra et al. [18] built and analyzed an ORC using a heat source at 120 °C and 110 °C with R245fa, R123, and mixtures of the two. They concluded that the highest thermal efficiency was from R123 at a thermal source temperature of 120 °C.

There are also reports of exergetic analyses of ORCs in charge of partially destroying the exergy of the residual currents of power generation systems, such as combined cycles. In these works, exergetic analyses are based on the application of Gouy Stodola's theorem and exergy balances; from these, the irreversibilities generated in the equipment and the exergetic efficiency of the generation systems expanded with ORCs are estimated. Nondy and Gogogi [19] carried out an exergy study in a combined cycle of a pressure level coupled to an ORC with R245fa as the working fluid. The ORC used, in a first configuration, the steam extracted from a turbine at 185 °C and, in a second configuration, the total steam flow leaving the turbine at the same temperature. The exergetic analysis revealed that the greatest irreversibilities of the ORC were located in the evaporator, with values higher than

2000 kW for both configurations followed by those of the turbine, regenerator, condenser, and pump. Jannatkhah et al. [20] designed a trigeneration system that took advantage of the waste heat of a diesel engine consisting of a heat exchanger for water heating, an ORC, and a refrigeration cycle that used R123 and ammonia. From the exergetic analysis, it was found that the exergetic efficiency of the system was 37.68% and that the lowest irreversibilities corresponded to the components of the ORC. Liao et al. [21] studied a cascade ORC that used R245fa, R600, R601a, and heptane as working fluids and took advantage of the thermal energy of combustion gases at 250 °C at a coal power plant. The exergetic efficiency of the complete system was calculated around 42% for the different working fluids of the ORC, and the study revealed that the best exergetic performance was obtained when using R601a and heptane. Boyaghchi and Montazerinejad [22] used flat-plate solar collectors to heat water with CuO particles. This solution at constant temperature was used as a thermal resource in an ORC for R245fa, R123, and R600a. They concluded that, for R123, the system presented the maximum exergetic efficiency corresponding to 38.61%, as well as the highest exergy destructions. Tiwari et al. [23] studied the behavior of an ORC in which a mixture of 10% heptane and 90% R245fa was evaporated by heat transfer with Therminol thermal oil that was heated in solar concentrators. The authors determined that the maximum exergetic efficiency was 14.38% and was associated with the maximum radiation. They also concluded that the greatest irreversibilities occurred in the evaporator, followed by the condenser, expander, and, finally, the pump.

Regarding working fluids, there are studies on a large number of refrigerants that have been analyzed by different authors under the same ORC configuration, proposing work output, thermal efficiency, power generation [24], and total heat transfer requirement [25] as performance indicators of energy analysis and exergetic efficiency and irreversibilities as indicators of exergetic analysis [26]. An ORC exergetic and exergoeconomic analysis reported R134a, R600a, R245fa, and R123 as viable refrigerants for these systems [27,28]. These refrigerants are not classified as environmentally friendly refrigerants, as they have zero ozone depletion potential ($ODP$ = 0), except for R123 ($ODP$ = 0.02); their global warming potentials ($GWP$s) are 1430, 1030, 77, and 5, for R134a, R245fa, R123, and R600a, respectively [29]. In this work, a thermodynamic analysis was carried out to compare the feasibility of using these four refrigerants in an ORC operation using as a residual thermal source the exhaust gases from the Hybrid Cycle Power Plant of the Valley of Mexico. The main configuration of the ORC for power generation was composed of a turbine, a condenser, a condensate pump, and a heat recovery steam generator (HRSG) consisting of an economizer, an evaporator, and a superheater. The power generation capacities of these systems ranged from 10 kW to around 20 MW [3]. This work is organized in three different sections. Section 2 presents the ORC description, followed by the energetic and exergetic analyses of the cycle. This section ends with a methodology to evaluate the use of a refrigerant in ORC operation based on the definition of an exergetic viability index of the refrigerant. Such viability contemplates the use of eight indicators that consider the generated power, the pinch point temperature difference, the unused exergy of the residual combustion gases, the specific steam consumption, the exergetic efficiency of the ORC, the total heat transfer requirement ($UA$) [25], the global warming potential ($GWP$), and the ozone depletion potential ($ODP$). Section 3 begins with a selection of 16 case studies (four for each refrigerant) based on the variation of evaporation and condensation temperatures as a function of the constant turbine inlet temperature using REFPROP 9.1 software [30]. Subsequently, a study of power generated from the influence of the temperature of the exhaust gases at the HRSG outlet of the ORC is carried out. Next, the irreversibilities generated in the OCR components and the global exergetic efficiency of the cycle are determined. Afterwards, the feasibility of using the four refrigerants in the ORC is analyzed from the indicators described above based on the variation of condensation temperature. Finally, Section 4 shows a conclusion of the refrigerants that are suitable to be used in the operation of the ORC.

In summary, the main contribution of our study is the proposal of an exergetic viability index that allows the selection of the best working fluid. This index, on the one hand, evaluates the influence of evaporation and condensation temperatures on the energy and exergy performance indicators of an ORC system and, on the other hand, combines these performance measures with two environmental indicators (*GWP* and *ODP*) and a structural indicator (*UA*).

## 2. Methodology

### *2.1. System Description*

ORCs are one of the most widely used technologies for power generation based mainly on low-temperature residual thermal energy sources. The operation of this cycle is based on the same principle as a Rankine cycle, but with an organic fluid instead of water vapor. Figure 1a shows the schematic diagram of an ORC composed of a pump ($Pump_1$) in charge of increasing the pressure of the refrigerant from the condenser pressure ($P_3$) to the turbine inlet pressure ($P_1 = P_4$). After the pumping process, the refrigerant was heated at constant pressure in an HRSG that took advantage of residual combustion gases, as seen in Figure 1b. In the HRSG, the temperature of the refrigerant increased from its compressed liquid temperature ($T_4$) to that of superheated steam ($T_1$) at the inlet of the turbine. The HRSG was made up of three main heat exchangers: an economizer (EC), an evaporator (EV), and a superheater (SH). Then, the superheated vapor of the refrigerant expanded in the turbine up to the condenser pressure (see process 1–2 of Figure 1b) and generated mechanical work. The turbine mechanically drove an electrical generator that generated electrical energy. Finally, the refrigerant was cooled isobarically in the condenser (see process 2–3 of Figure 1b) to a saturated liquid condition by means of exchanging heat with a water flow that came from the cooling tower.

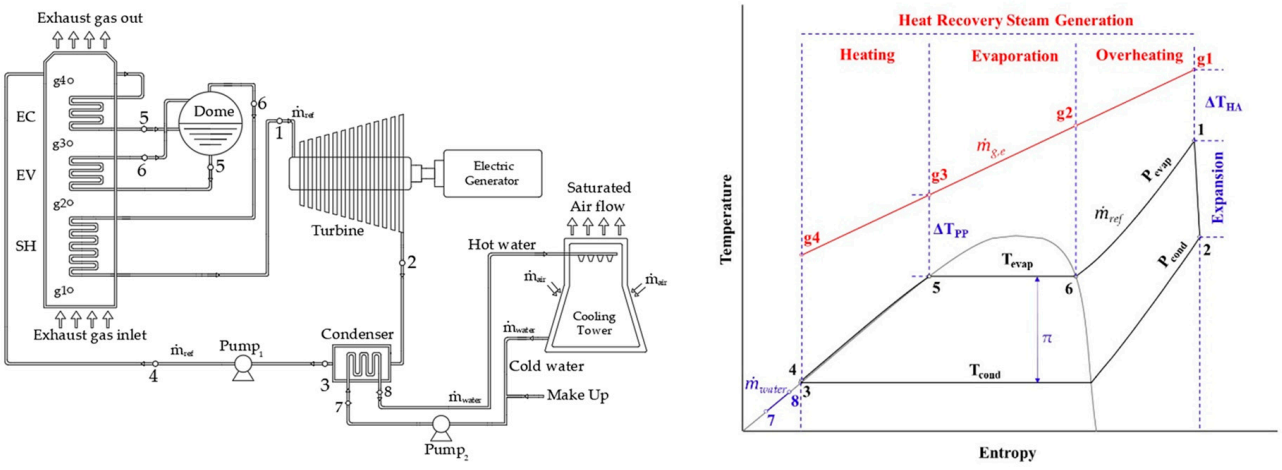


**Figure 1.** ORC plant of case study: (**a**) Schematic diagram and (**b**) temperature–entropy diagram of the ORC.

Residual thermal source came from the combustion gases of the HRSG at the Hybrid Cycle Power Plant of the Valley of Mexico operating at full load. Exhaust gas flow was generated by the joint operation of the gas turbines. In this work, it was considered that the temperature of the exhaust gases at the chimney of the HRSG of the hybrid cycle was the same as at the HRSG inlet of the ORC, i.e., the heat losses of the exhaust gases when entering the HRSG of the ORC were neglected.

A hot water flow was fed to the cooling tower and cooled by convection heat transfer with fan-induced atmospheric air flow. The heated humid air flow left the tower with a rel-

ative humidity of 100%, and to compensate for the water entrainment into the environment by the air, the water flow was replenished ($\dot{m}_{make\ up}$).

### 2.2. Energy Analysis

The mass and energy balances of the ORC were carried out under the following assumptions:

1. The ORC operated in a steady state;
2. The pump and turbine were considered adiabatic;
3. The properties of water and refrigerants were estimated using REFPROP 9.1 software [30].
4. The exhaust gases behaved as an ideal gas mixture with a heat capacity at invariant constant pressure at the temperature of $c_{pg}$ = 1.288 kJ/kg K;
5. The kinetic and potential energy changes of refrigerants, water, and combustion gases were negligible;
6. The temperature and pressure of the dead state were $T_0 = T_{amb}$ and $P_0 = P_{atm}$, respectively.

In this work, the following input parameters for the ORC energy model were considered:

7. The temperature and pressure of the environment ($T_{amb}$ and $P_{atm}$);
8. The hot approach temperature differences defined by $\Delta T_{HA} = T_{g1} - T_1$, to determine the refrigerant temperature at the SH outlet ($T_1$);
9. The temperature of the exhaust gases at the HRSG inlet ($T_{g1}$);
10. The mass flow of the exhaust gases ($\dot{m}_g$);
11. The temperature of the exhaust gases at the outlet of the HRSG chimney ($T_{g4}$), which must be greater than or equal to 100 °C to avoid condensation of water contained in the exhaust gases. This temperature was used to quantify the mass flow of refrigerant in the cycle;
12. The evaporation temperature of the refrigerant ($T_{evap}$), which must be lower than its critical temperature;
13. The difference between the temperature of the refrigerant in the condenser and the ambient temperature, $\Delta T_{cond} = T_{cond} - T_{amb}$, which was used to establish the condensing temperature of the refrigerant;
14. The temperature difference between the water at the outlet and inlet of the condenser, $\Delta T_{water} = T_8 - T_{amb}$, which calculated the temperature of the water at the outlet of the equipment ($T_8$);
15. The isentropic efficiencies of the turbine ($\eta_{IT}$) and the pump ($\eta_{IP}$) were assumed to be constant.

From the energy balance in the turbine, the work generated was obtained, and a part of it was used to feed the pump in such way that the work output generated by the ORC is:

$$w_m = (h_1 - h_2) - (h_4 - h_3) \quad (1)$$

The heat transferred from the exhaust gases to a mass unit of refrigerant in the HRSG is given by:

$$q_{\text{sup}} = (h_1 - h_4) \quad (2)$$

In the condenser, the working fluid was cooled by transferring heat to the cooling water. The heat rejected by the refrigerant is:

$$q_{rej} = (h_2 - h_3) \quad (3)$$

The thermal efficiency of the cycle was calculated as the ratio between the work output generated by the cycle and the heat supplied to the refrigerant in the HRSG:

$$\eta_{th} = \frac{w_m}{q_{\text{sup}}} \quad (4)$$

The mass flow of the working fluid was determined by means of an energy balance in the HRSG as a function of the total heat flow released by the exhaust gases and the total heat flow used by the working fluid:

$$\dot{m}_{ref} = \frac{\dot{m}_g c_{p_g} \left[T_{g1} - T_{g4}\right]}{(h_1 - h_4)} \tag{5}$$

Equation (5) is restricted by the pinch point temperature difference parameter, which concerns the EV of the HRSG and corresponds to the difference between the temperature of the exhaust gases at the outlet of the evaporator and the evaporation temperature of the refrigerant, $\Delta T_{PP} = T_{g3} - T_{evap}$, which must be greater than 5 °C.

Therefore, motor power generated by the cycle was calculated as the product of the mass flow of the working fluid and the work output generated:

$$\dot{W}_m = \dot{m}_{ref}\, w_m \tag{6}$$

The cooling water mass flow required to absorb the heat flow rejected by the refrigerant in the condenser is:

$$\dot{m}_{water} = \frac{\dot{m}_{ref}(h_2 - h_3)}{(h_8 - h_7)} \tag{7}$$

The heat rate is the amount of energy needed to generate one kWh and is given by:

$$HR = \frac{3600}{\eta_{th}} \tag{8}$$

The specific steam consumption ($SSC$) is the mass of refrigerant required to generate one kWh of energy:

$$SSC = \frac{3600\ \dot{m}_{ref}}{\dot{W}_m} \tag{9}$$

### *2.3. Analysis of the Second Law of Thermodynamics*

The mathematical formulation of the Second Law of Thermodynamics for open systems is:

$$\left(\frac{dS}{dt}\right)_{vc} + \sum \dot{m}_{out} s_{out} - \sum \dot{m}_{int} s_{int} = \sum \frac{\dot{Q}_i}{T_i} + \dot{S}_{gen} \tag{10}$$

The entropy production in the ORC components is presented in Table 1 and was obtained from Equation (10), assuming that the system operates in a steady flow and that the components are adiabatic.

**Table 1.** Entropy generated by the ORC components.

| Component | Generated Entropy |
|---|---|
| Heat recovery steam generator *(HRSG)* | $\dot{S}_{gen_{CRC}} = \dot{m}_g \left[c_{p_g} \ln\left(\frac{T_{g4}}{T_{g1}}\right)\right] + \dot{m}_{ref}(s_1 - s_4)$ |
| Turbine *(T)* | $\dot{S}_{gen_T} = \dot{m}_{ref}(s_2 - s_1)$ |
| Pump *(P)* | $\dot{S}_{gen_B} = \dot{m}_{ref}(s_4 - s_3)$ |
| Condenser *(COND)* | $\dot{S}_{gen_{COND}} = \dot{m}_{ref}(s_3 - s_2) + \dot{m}_{agua}(s_{out} - s_{out})$ |

From Gouy Stodola's theorem, it follows that the irreversibilities of the ORC components are related to their entropy generated according to:

$$\dot{I}_i = T_0 \dot{S}_{gen_i},\ i\ =\ HRSG,\ T,\ P,\ COND \tag{11}$$

where $T_0$ is the temperature of the dead state.

The exergy of a stream is the maximum amount of work available that can be obtained when it is brought to the dead state by means of reversible processes. The exergy of a stream in the absence of magnetic, electrical, and nuclear interactions is composed by its physical, chemical, kinetic, and potential exergy. As an ORC involves only physical processes and the kinetic and potential energy changes of the fluids are neglected, then the only contribution to the total exergy of the fluids is the physical exergy given by:

$$\dot{E}_j^{ph} = \dot{m}_k\left[\left(h_j - h_0\right) - T_0\left(s_j - s_0\right)\right],\ k\ =\ \text{water and refrigerant.} \tag{12}$$

When modeling exhaust gases as ideal gases, from Equation (12) and the equation of the state for an ideal gas, it is evident that the physical exergy of exhaust gases can be expressed as follows:

$$\dot{E}_j^{ph} = \dot{m}_g\left[\left(h_j - h_0\right) - T_0\left(c_{p_g}\ln\frac{T_j}{T_0} - R_g\ln\frac{P_j}{P_0}\right)\right],\ j\ =\ g1,\ \ldots,\ g4 \tag{13}$$

Therefore, the exergy efficiency of an ORC can be determined based on the ratio between the sum of the flow of internal irreversibilities generated by each of the process equipment with respect to the exergy flow of the exhaust gases that pass through the HRSG, which can be obtained using the following expression:

$$\eta_{exer} = 1 - \frac{\sum \dot{I}_i}{\dot{E}_{g1}^{ph}} \tag{14}$$

### *2.4. Evaluation of the Exergetic Feasibility of the Use of the Refrigerant in the ORC*

In this section, to evaluate the viability of using a refrigerant to generate power in an ORC taking advantage of a residual thermal source of combustion gases, the exergetic viability index of the refrigerant is defined and denoted by $\xi_{ref}$. This index, defined by Equation (15), is the weighted average of the indicators presented in Table 2 ($\alpha_i$):

$$\xi_{refrigerant} = \sum_{i=1}^{8} \omega_i \alpha_i. \tag{15}$$

where $\omega_i$ is the main factor of the $i$-th indicator, and the sum of all these factors is equal to unity, which is $\sum_{i=1}^{8} \omega_i = 1$. It is worth mentioning that the refrigerant with the highest exergetic viability is the one that has the highest value of the exergetic viability index.

Among the indicators used to define the exergetic viability index are the power generated by the ORC, ($\Delta T_{PP}$), the unused exergy of the residual combustion gases, the *SSC*, the exergetic efficiency, the *GWP*, and the *ODP* of the ORC. In addition to these energy, exergetic, and environmental indicators, this work included the total heat transfer requirement $(UA)_{tot}$ as a structural indicator of the systems. The total heat transfer requirement provides an estimate of the total heat transfer area of the heat exchangers in the ORC, assuming that the heat transfer coefficient differences of the refrigerants are negligible [25]. This indicator can be computed from the following equation [31–33]:

$$(UA)_{tot} = \sum \frac{\dot{Q}_i}{\Delta T_m} = \frac{\dot{Q}_{EC}}{\Delta T_{m,EC}} + \frac{\dot{Q}_{EV}}{\Delta T_{m,EV}} + \frac{\dot{Q}_{SH}}{\Delta T_{m,SH}}, \tag{16}$$

where $\Delta T_m$ is the logarithmic mean temperature difference.

**Table 2.** Exergetic viability index of refrigerant.

| Indicator | Expression | Range | Weighting Factor |
|---|---|---|---|
| Power $\alpha_1 = \alpha_{\dot{W}_m}$ | $\alpha_{\dot{W}m} = \frac{\dot{W}_m}{\dot{W}_{m,max}} 100$ where $\dot{W}_{m,max}$ is the maximum power of all the case studies. $\dot{W}_m$ is the power of the case study to be evaluated. | $0 \leq \alpha_{\dot{W}m} \leq 100$ Values of $\alpha_{\dot{W}_m}$ close to 100 indicate that high powers are being generated compared to the other case studies. | $\omega_1 = 0.141$ |
| Pinch point temperature difference $\alpha_2 = \alpha_{\Delta T_{PP}}$ | $\alpha_{\Delta T_{PP}} = \begin{cases} 40, & \text{if } 0 < \Delta T_{PP} < 10 \\ 100, & \text{if } 10 \leq \Delta T_{PP} \leq 20 \\ 60, & \text{if } 20 < \Delta T_{PP} \leq 30 \\ 50, & \text{if } \Delta T_{PP} > 30 \end{cases}$ | $40 \leq \alpha_{\Delta T_{PP}} \leq 100$ Values of $\alpha_{\Delta T_{PP}}$ close to 100 indicate that $\Delta T_{PP}$ are within the established range and correspond to values reported in the literature. [34–37]. | $\omega_2 = 0.141$ |
| Residual exhaust gases exergy flow $\alpha_3 = \alpha_{\Delta \dot{E}_{g4-g0}}$ | $\alpha_{\Delta \dot{E}_{g4-g0}} = \left(1 - \frac{\Delta \dot{E}_{g4-g0}}{\Delta \dot{E}_{g4-g0,max}}\right) 100$ | $0 \leq \alpha_{\Delta \dot{E}_{g4-g0}} \leq 100$ Values of $\alpha_{\Delta \dot{E}_{g1-g0}}$ close to 100 indicate the highest exergy amounts of heat transferred from the residual combustion gases to the environment. | $\omega_3 = 0.141$ |
| Specific steam consumption $\alpha_4 = \alpha_{SSC}$ | $\alpha_{CEV} = \left(1 - \frac{SSC}{SSC_{max}}\right) 100$ | $0 \leq \alpha_{SSC} \leq 100$ Values of $\alpha_{SSC}$ close to 100 indicate the smallest amounts of refrigerant mass flow required to generate one kWh. | $\omega_4 = 0.141$ |
| Exergy efficiency $\alpha_5 = \alpha_{\eta_{exer}}$ | $\alpha_{\eta_{exer}} = \frac{\eta_{exer}}{\eta_{exer,max}} 100$ where $\eta_{exer,max}$ is the maximum exergetic efficiency of all the case studies. $\eta_{exer}$ is the exergetic efficiency of the case study to be evaluated. | $0 \leq \alpha_{\eta_{exer}} \leq 100$ Values of $\alpha_{\eta_{exer}}$ close to 100 indicate the highest exergetic efficiencies compared to the case studies. | $\omega_5 = 0.141$ |
| Total heat transfer requirement $\alpha_6 = \alpha_{UA}$ | $\alpha_{(UA)_{tot}} = \left[1 - \frac{(UA)_{tot}}{(UA)_{max}}\right] 100$ where $(UA)_{max}$ is the maximum total heat transfer requirement of all the case studies and $(UA)_{tot}$ is the total heat transfer requirement of the case study to be evaluated see Equation (16). | $0 \leq \alpha_{UA} \leq 100$ Values of $\alpha_{UA}$ close to 0 indicate the smallest heat transfer requirement compared to the case studies. | $\omega_6 = 0.141$ |
| Global warming index $\alpha_7 = \alpha_{GWP}$ | $\alpha_{GWP} = \left(1 - \frac{\frac{\dot{m}_{ref} GWP}{\dot{W}_{net}}}{\frac{\dot{m}_{R134a,max} GWP_{R134a}}{\dot{W}_{net@\dot{m}_{R134a,max}}}}\right) 100$ where $GWP$ is the global warming potential of the refrigerant in the case study. The case study corresponding to the R134a refrigerant with the highest mass flow was taken as the base case, since this was the refrigerant with the highest value of $GWP$ = 1430 $g_{CO2}/kg_{R134a}$ [17,38]. | $0 \leq \alpha_{GWP} \leq 100$ Values of $\alpha_{GWP}$ close to 100 indicate the largest contributions to the $GWP$. | $\omega_7 = 0.10$ |
| Ozone depletion potential $\alpha_8 = \alpha_{ODP}$ | $\alpha_{ODP} = \left(1 - \frac{ODP}{ODP_{max}}\right) 100$ where $ODP$ is the ozone depletion potential of the refrigerant in the case study. The case study corresponding to the R123 refrigerant with the highest $ODP$ value was taken as the base case [29]. | $0 \leq \alpha_{ODP} \leq 100$ Values of $\alpha_{ODP}$ close to 100 indicate the smallest contributions to the $ODP$. | $\omega_8 = 0.05$ |

## 3. Results and Discussion

The energy and exergy studies of the ORC for the organic fluids R134a, R600a, R245fa, and R123 were carried out considering the operating conditions in Table 3.

**Table 3.** ORC operating conditions.

| Operating conditions | | | | | | | |
|---|---|---|---|---|---|---|---|
| **Environment** | | **Organic Fluid** | | **Residual Thermal Source** | | **Cooling Water** | |
| $P_{atm}$, (bar) | 0.78 | $\Delta T_{HA}$, (°C) | 35 | $T_{g1}$, (°C) | 185 | $\Delta T_{water}$, (°C) | 10 |
| $T_{amb}$, (°C) | 10 a 40 | $\Delta T_{cond}$, (°C) | 15 | $T_{g4}$, (°C) | ≥100 | $T_7$, (°C) | $T_{amb}$ |
| | | $\eta_{IT}$, (-) | 0.90 | $\dot{m}_g$ ($kg_g/s$) | 297.1 | $P_7$, (bar) | $P_{atm} + \Delta P_{water}$ |
| | | $\eta_{IB}$, (-) | 0.80 | | | $\Delta P_{water}$, (bar) | 0.2 |

### *3.1. Selection of Case Studies Based on a Residual Thermal Source*

An ORC can only operate if the evaporation temperature of the refrigerant is between the condensation temperature and the critical temperature of the refrigerant ($T_{cond} < T_{evap} < T_{crit}$), as seen in Figure 1b. This restriction of temperatures has its counterpart in pressures, i.e., the existence of the cycle is subject to the evaporation pressure being limited by the condensation pressure and the critical pressure ($P_{cond} < P_{evap} < P_{crit}$). If $\pi$ is defined as the ratio of evaporation and condensation pressures of the refrigerant in an ORC (see Equation (17)), then for the thermodynamic cycle to be functional, this relationship must satisfy that $1 < \pi < P_{crit}/P_{cond}$. It is worth mentioning that, if the evaporation and condensation temperatures are both close to the critical point, the cycle loses its productive purpose, which consists of taking advantage of the thermal energy from residual sources at low temperatures. At the other extreme, if evaporation and condensation temperatures are close, then low power generation makes the conception of the cycle absurd.

$$\pi = \frac{P_{evap@T_{evap}}}{P_{cond@T_{cond}}} \tag{17}$$

In this work, the performance of an ORC operating with four refrigerants (R134a, R600a, R245fa, and R123) was studied, and to evaluate the influence of a large number of combinations of evaporation and condensation temperatures on its performance, a parametric analysis of the work output of the cycle as a function of these temperatures was carried out. In this analysis, condensation temperature was swept from 25 °C to 55 °C for the four refrigerants, while the evaporation temperatures were higher than the condensation temperature and lower than the critical temperature. Thus, the evaporation temperature ranged from 75 °C for all refrigerants and up to 95 °C for R134a, 134 °C for R600a and 142 °C for R245fa and R123. In this temperature range, the evaporation ratio and condensation pressures were first calculated, and then the energy model for the refrigerant in the ORC was solved to determine the specific work output ($w_m$ given by Equation (1)) generated.

Figure 2 shows the parametric behavior of the work output as a function of the evaporation and condensation pressure ratio for each of the refrigerants in the aforementioned evaporation and condensation temperature ranges. This figure shows, that, for a given evaporation temperature, the work output decreased with the condensation temperature and increased with the pressure ratio. On the other hand, for a constant condensation temperature, the work output increased with the evaporation temperature until reaching a maximum; however, the temperature associated with this condition was close to the critical temperature. The work output presented the same behavior with respect to the pressure ratio, keeping the condensation temperature fixed. These observations can be seen in Figure 2b,c, which show that, at evaporation temperatures of 129 and 138 °C, the R600a and R245fa refrigerants reached maximum work output, respectively. When these temperatures were exceeded, their behavior became decreasing for any condensation temperature value between 25 and 55 °C.

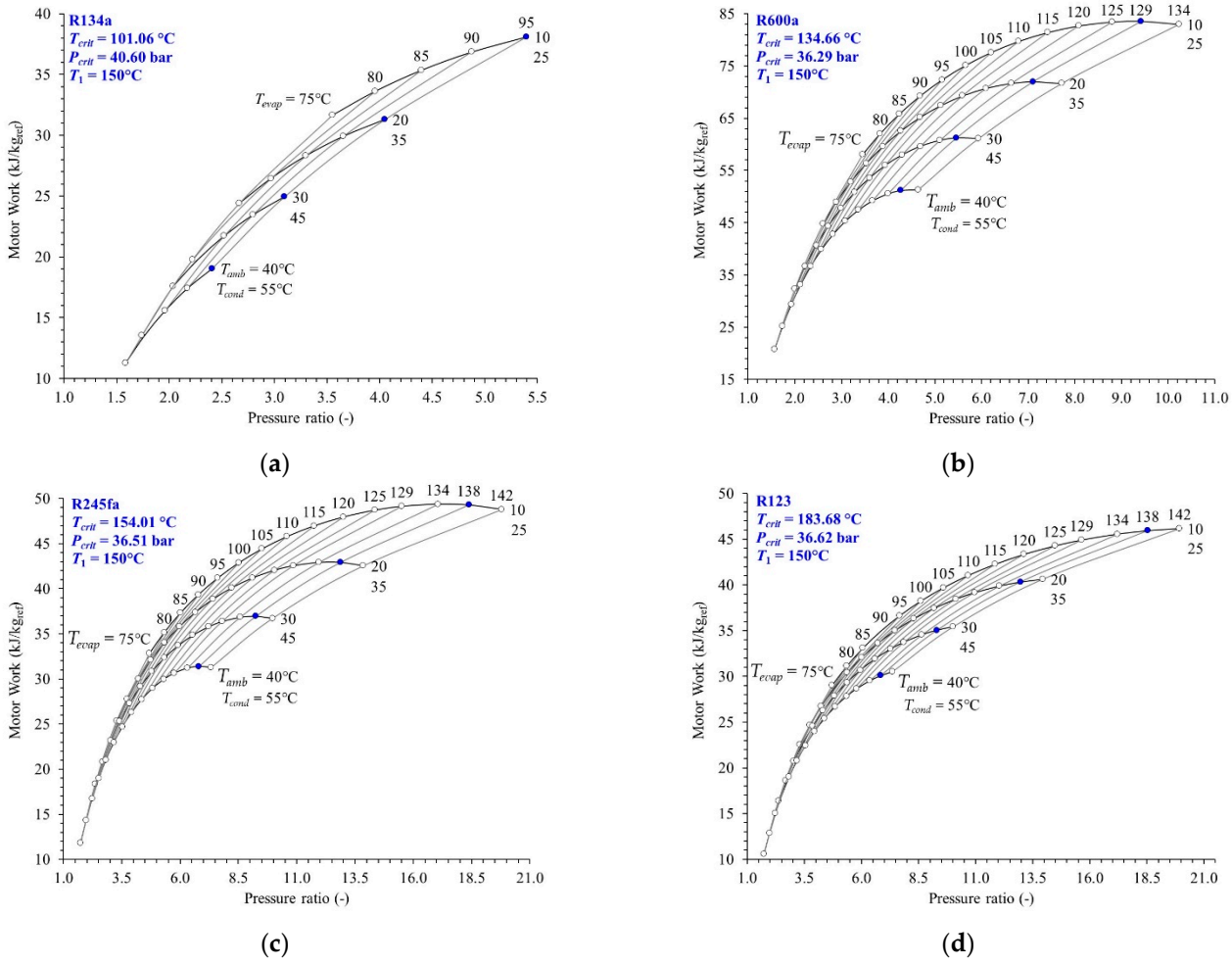


**Figure 2.** Work output as a function of the pressure ratio for different ambient temperatures: (**a**) R134a, (**b**) R600a, (**c**) R245fa, and (**d**) R123.

Figure 2 also shows that the work output obtained with the R134a refrigerant was greater than that generated by R123, as long as the evaporation temperature was far from the critical temperature of R134a. However, as the evaporation temperature tended toward the critical temperature of R134a, the work output generated by the use of both refrigerants tended toward the same value; this behavior was accentuated at condensation temperatures greater than 45 °C. For evaporation temperatures between 75 and 95 °C, the work output for the different refrigerants satisfied the inequality $w_{m,\,\mathrm{R600a}} > w_{m,\,\mathrm{R245fa}} > w_m$, R134a > $w_{m,\,\mathrm{R123}}$, while, for evaporation temperatures between 95 and 129 °C, it was fulfilled that $w_{m,\,\mathrm{R600a}} > w_{m,\,\mathrm{R245fa}} > w_{m,\,\mathrm{R123}}$. Finally, for evaporation temperatures between 129 and 138 °C, it was satisfied that $w_{m,\,\mathrm{R245fa}} > w_{m,\,\mathrm{R123}}$. This behavior of work output was directly related to the pressure ratio; for example, the R245fa and R123 refrigerants exhibited similar pressure ratios for different combinations of evaporation and condensation temperatures, and their work outputs differed on average at 4.19, 3.31, 2.52, and 1.83 kJ/kg for condensation temperatures of 25, 35, 45, and 55 °C, respectively (see Figure 2c,d). Furthermore, at a given evaporation temperature, the difference between the work output generated by the refrigerants decreased as the condensation temperature increased.

Derived from above, the evaporation and condensation temperature space was wide. For this reason, in this work, the thermodynamic study was carried out for 25, 35, 45, and 55 °C condensation temperatures on all refrigerants with a 95 °C evaporation temperature for R134a, 129 °C for R600a, and 138 °C for the R245fa and R123 fluids (blue points in Figure 2). The 16 case studies chosen (four for each refrigerant) have associated work

outputs close to their maximum values (see Table 2) and evaporation and condensation pressure ratios greater than one (see Table 2) for all refrigerants. In addition:

1. For R134a and R600a, the evaporation temperatures were close to their respective critical temperatures, 101.6 and 134.66 °C, which in turn were lower than the steam temperature;
2. For R245fa and R123, the same evaporation temperature was taken, which was far from both critical temperatures, 154.01 and 183.68 °C, which were higher than the turbine inlet temperature. On the other hand, this allowed analysis of the impact of the nature of the fluid on the heat transferred in the SH.

According to Table A1 (Appendix A), when comparing the four case studies regarding the same refrigerant and the same evaporation temperature, it resulted that both the work output and the heat supplied per unit mass of the refrigerant decreased with the condensation temperature. This behavior was such that the thermal efficiency also decreased with the condensation temperature.

For the same condensing temperature, as mentioned above, the refrigerants generated the greatest amount of work output for different evaporation temperatures. Under these conditions, the heat that must be supplied per unit mass of the refrigerant was greater for R600a, followed by R245fa, R134a, and R123. This fact is directly related to the opening of the saturation bell in a temperature–entropy diagram, i.e., the greater the entropy change of the refrigerant in the HRSG, the greater the heat that the refrigerant must absorb to reach the turbine inlet temperature. Consequently, for a constant condensing temperature, it was discovered that the thermal efficiency satisfies the following order relation: $\eta_{th,\ 123} > \eta_{th,}$ 245fa $> \eta_{th,\ 600a} > \eta_{th,\ 134a}$. *HR* and thermal efficiency are inversely proportional energy indicators, and Table 2 indicates that thermal energy between 19,000 and 44,000 kJ was required to generate one kWh of work output in the 16 cases.

### *3.2. Influence of the Temperature of the Combustion Gases at the HRSG Outlet of the ORC on the Power and Refrigerant Flow*

In this section, the refrigerant flow was analyzed for power generation in an ORC that took advantage of the energy contained in the residual combustion gases at $T_{g1}$ = 185 °C from the HRSG at the Hybrid Combined Cycle Power Plant of the Valley of Mexico. This analysis was carried out for the 16 case studies established in the previous section for a temperature range of residual gases at the outlet of the HRSG from $T_{g4}$ = 170 to 100 °C. The lower limit of the selected range for $T_{g4}$ was greater than the dew point temperature of gases at atmospheric pressure. Figure 3 presents the relationship between cycle power and refrigerant mass flow using a constant condensing temperature (and, hence, constant evaporating and condensing pressure ratios, since evaporating temperature is fixed for each refrigerant) and residual exhaust gas outlet temperature as parameters. This figure shows that, for each refrigerant, the highest powers were obtained at low $T_{g4}$ values, which was indicative of a better use of residual thermal energy. On the other hand, the refrigerant mass flow at constant $T_{g4}$ increased with the condensing temperature at the same time that power generation was disfavored. When comparing the influence of $T_{g4}$ on the power generated for the four different refrigerants used in the ORC, the result was that an increase of 1 °C in $T_{g4}$ while keeping constant condensation and evaporation temperatures made the power losses more important for R123, followed by R245fa, R600a, and R134a (for $T_{cond}$ = 25 °C, $\Delta\dot{W}_{R123} = -72.21$ kW $< \Delta\dot{W}_{R245fa} = -68.07$ kW $< \Delta\dot{W}_{R600a} = -63.58$ kW $< \Delta\dot{W}_{R134a} = -52.84$ kW). In addition, it led to a decrease in the mass flow of the refrigerants in the following order, with R123 being the most impacted, followed by R134a, R245fa, and R600a (for $T_{cond}$ = 25 °C, $\Delta\dot{m}_{R123} = -1.57$ $kg_{ref}/s < \Delta\dot{m}_{R134a} = -1.39$ $kg_{ref}/s < \Delta\dot{m}_{R245fa} = -1.38$ $kg_{ref}/s < \Delta\dot{m}_{R600a} = -0.76$ $kg_{ref}/s$). For $\Delta T_{g4}$ = 1 °C, power losses and refrigerant mass flow decreases were lower with increased condensing temperature.

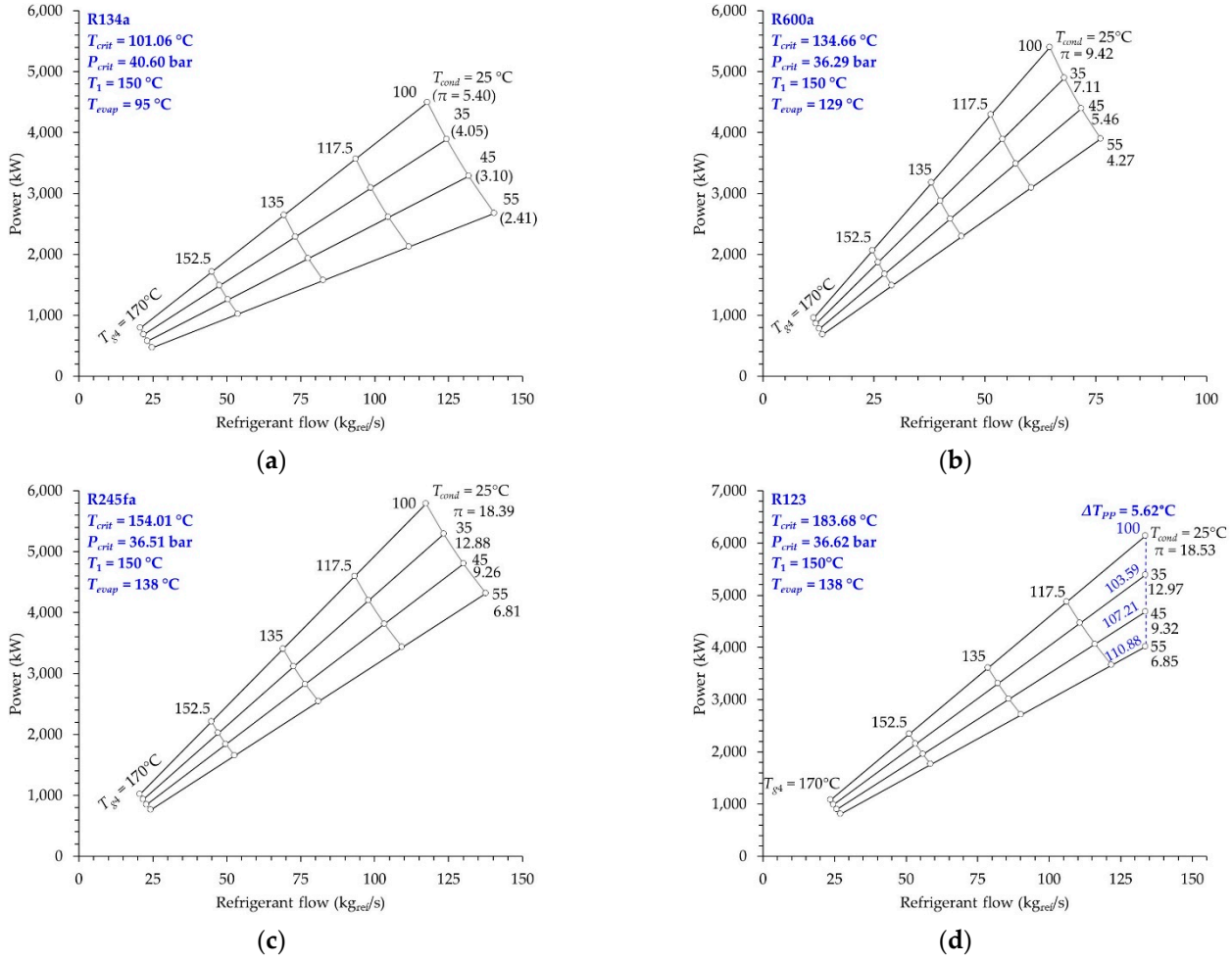


**Figure 3.** Power generation as a function of the refrigerant mass flow for different pressure ratio conditions, and the variation of exhaust gas temperature at the HRSG outlet for the different refrigerants: (**a**) R134a, (**b**) R600a, (**c**) R245fa, and (**d**) R123.

It is important to note that, for the case of Figure 3d corresponding to refrigerant R123, and for $T_{g4}$ = 100 °C, it was not possible to generate power for the condensation temperatures studied because $\Delta T_{PP}$ was very close to 0 °C or negative. For this reason, for this refrigerant, the temperature corresponding to $\Delta T_{PP}$ = 5.62 °C was taken as the lower limit for $T_{g4}$. Of the refrigerants studied, R123 was the fluid that allowed the highest power to be generated at condensing temperatures between 25 and 45 °C, while R245fa, at a condensing temperature of 55 °C, was the refrigerant that generated the greatest power.

In Table A2 of Appendix A, the power variation is presented as a function of the increase in the ambient temperature of constant exhaust gas temperature for the working fluids R134a, R600a, and R245fa, while $\Delta T_{PP}$ was constant for R123. It can be seen that the refrigerant mass flow rate increased when the ambient temperature increased, and this represented a decrease in $\Delta T_{PP}$. The R600a fluid showed the highest amount of work output (see Figure 2b); however, it also showed the lowest amounts of mass flow and, therefore, did not necessarily generate the highest amounts of power. The R134a and R245fa fluids showed a similarity in mass flow, but with a 1300 kW difference in the power generated. In addition, the heat flow rejected in the condenser was above 25,000 kW, and this resulted in using large amounts of cooling water flow. In contrast, the R245fa and R123 fluids showed a similar behavior in the number of $kg_{ref}$ needed to produce one kWh, while the R600a fluid showed a decrease between 30 and 40 $kg_{ref}$ to produce the same kWh.

### *3.3. Analysis of the Second Law of Thermodynamics*

This section presents the results of the analysis of the Second Law of Thermodynamics applied to the ORC for the four refrigerants and the sixteen operating conditions shown in Table A2. The irreversibilities generated in the ORC components for the four refrigerants are shown in Figure 4 for $T_{g4}$ = 100 °C; $T_{cond}$ = 25, 35, 45, and 55 °C; and $\Delta T_{PP}$ = 5.62 °C. When comparing the irreversibilities of the ORC components by refrigerant, it was observed that R134a and R123 present, respectively, the highest and lowest irreversibilities for the different condensation temperatures. For each refrigerant, it was also seen that increasing the condensing temperature from 25 to 55 °C produced an average decrease in the irreversibilities of 180, 283, 297, and 319 kW for R134a, R600a, R245fa, and R123, respectively. For the 16 case studies, the HRSG components of the ORC, in which the transfer of residual combustion gases to the refrigerant occurs, together destroyed the greatest amount of exergy in the following order: EC, EV, and SH. The condenser, responsible for refrigerant condensation by removing heat from the cooling system, was the second component to generate the highest irreversibilities. Finally, the turbine and the refrigerant circuit pump were the components that destroyed the least amounts of exergy. All these results are presented in Table A3 (Appendix B).

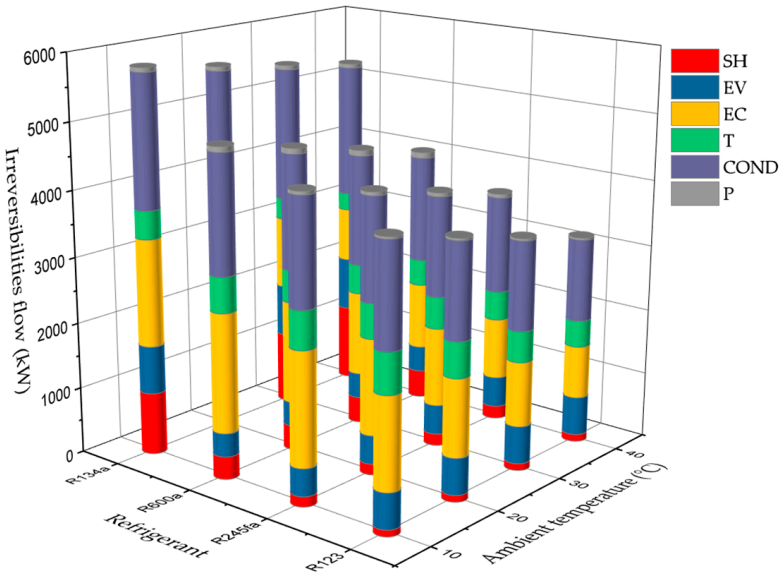


**Figure 4.** Flow of irreversibilities of the ORC components as a function of the condensation temperature for the different refrigerants (R134a, R600a, R245fa, and R123); $T_{g1}$ = 185°C, $T_{g4}$ = 100 °C, and $\Delta T_{PP}$ = 5.62 °C for R123.

The HRSG irreversibilities were analyzed by a Carnot factor profile as a function of heat exchange between the refrigerant and residual combustion gases in each sections of such a component, as shown in Figure 5. The area under the Carnot factor profile of the combustion gases (red line in Figure 5) corresponds to the exergy associated with the heat transferred by this working fluid to modify its thermodynamic state ($g_i$ to $g_{i+1}$; $i$ = 1, 2, 3 and 4). Similarly, the area under the Carnot factor profile of the refrigerant is the exergy associated with the heat that the refrigerant can absorb to fulfill its productive purpose. The difference between these areas (shaded region) is a measure of exergy wastage contained in the residual combustion gases by the refrigerant. It should be noted that the smaller the difference in areas, the greater the use of the exergy contained in the residual combustion gases. This use is limited by the nature of the refrigerant, waste heat source, life cycle costs of the ORC, space constraints, and design parameters, such as $\Delta T_{PP}$. As not all the exergy of the residual combustion gases is used to increase the exergy of the refrigerant up to state 1, then, the remaining exergy in the exhaust gases is removed to the environment.

This residual exergy of the exhaust gases is waste, and in Figure 5 corresponds to the area under the curve of the Carnot profile section of the exhaust gases from state $g_4$ a $g_0$.

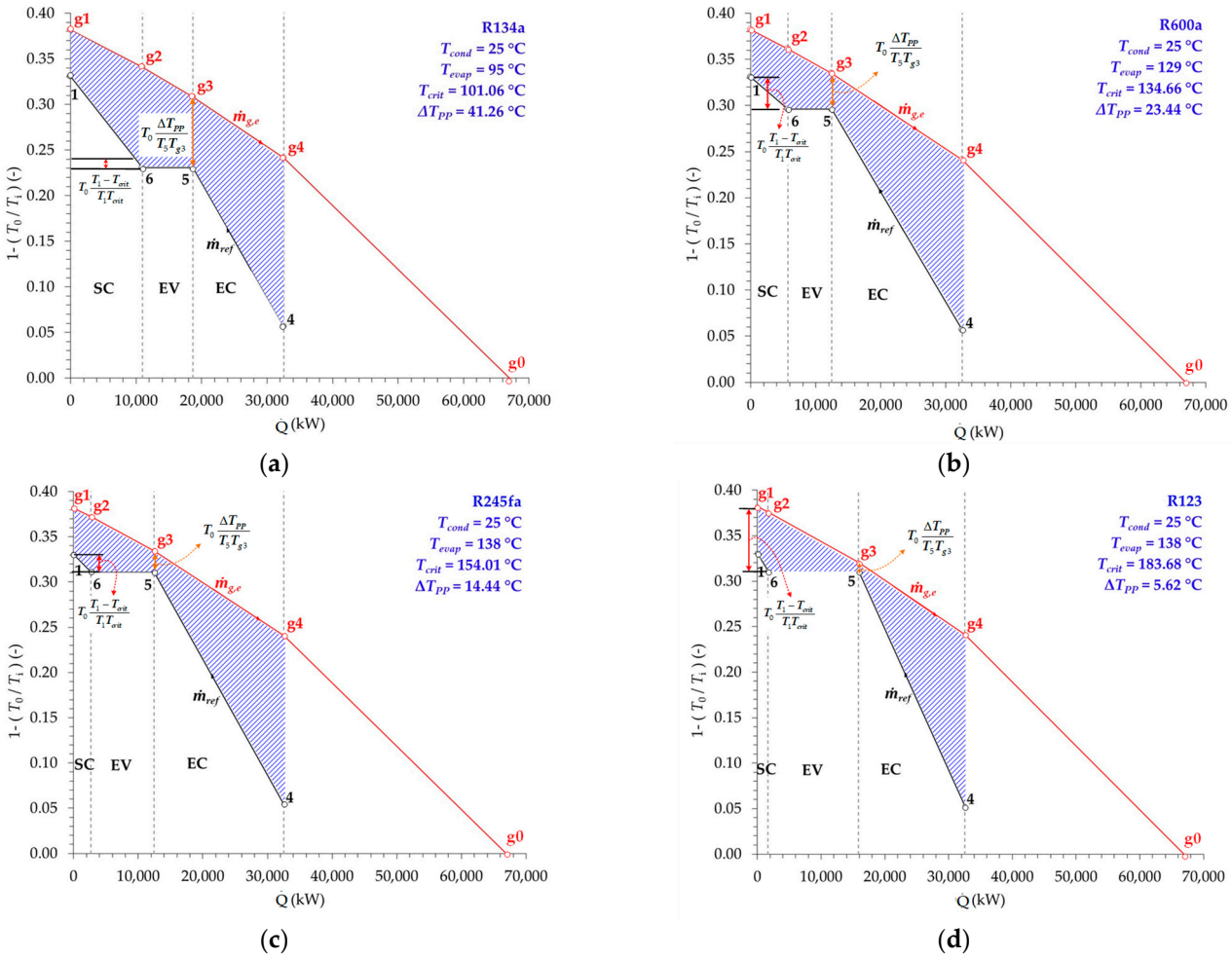


**Figure 5.** Exergy profiles of the HRSG components of the ORC for the different working fluids: (**a**) R134a, (**b**) R600a, (**c**) R245fa, and (**d**) R123.

Figure 5 presents the profiles of the Carnot cycle as a function of the heat transferred in each of the stages of the HRSG of the ORC operating with the R134a, R600a, 245fa, and R123 refrigerants at a $T_{cond}$ = 25 °C condensing temperature and an exhaust gas temperature of $T_{g4}$ = 100 °C. In all cases, the EC was the section of the HRSG that generated the largest irreversibilities. However, this figure reveals that the exergy destroyed in this subcomponent was highly sensitive to the difference in Carnot factors associated with state 5 of the refrigerant and $g_3$ of the residual combustion gases (see orange line in Figure 5). This difference was proportional to $\Delta T_{PP} = T_{g3} - T_5$, according to $T_0/(T_5\ T_{g3})\ \Delta T_{PP}$: as $\Delta T_{PP}$ decreased, the irreversibilities generated in the EC also decreased, which induced a reduction in irreversibilities in the EV. This fact can be seen when comparing Figure 5a,b corresponding to the refrigerants R134a and R600a, respectively. $\Delta T_{PP}$ in the EV of the ORC operating with R600a was lower than with R134a, and, therefore, the EV with R134a generated more irreversibilities than with R600a.

The comparison of the Carnot factor profiles in the HRSG for the different refrigerants indicated that the critical point of these fluids is also a parameter that mainly influences the exergy destruction in the SH. The critical temperature is the upper bound of the refrigerant evaporation temperature ($T_6 = T_{evap}$). In this way, on the one hand, if $T_1 > T_{crit}$, then as $T_6$ approaches $T_1$, the irreversibility of the SH decreases, which can be observed when

comparing Figures 5a and 5b. On the other hand, if $T_1 < T_{crit}$ then $T_6$ can take the value of $T_1$, as long as $\Delta T_{PP} > 0$; while $T_6$ is closer to $T_1$, the irreversibility in the SH decreases. This fact gives the possibility that the existence of the SH is unnecessary and $T_1 < T_{crit}$, $T_1 \approx T_6$, and $\Delta T_{PP} > 0$.

From the above observations, it was evident that the greatest irreversibilities generated in the SH were obtained by the use of R134a and R600a because their critical temperatures were lower than $T_1$ and $(T_1 - T_6)_{\text{R134a}} > (T_1 - T_6)_{\text{R600a}}$. On the other hand, for Figure 5c,d, the evaporation temperature was the same ($T_6 = T_{evap} = 138$ °C). In addition, the critical temperatures of R245fa and R123 were greater than $T_1$, and $T_{crit,\text{R123}} > T_{crit,\text{R245fa}}$, which caused the irreversibility of the SH to be lower for R123 compared to R245fa.

A Grassmann diagram is a graphical representation to visualize the results of an analysis of the Second Law of Thermodynamics. These diagrams show the exergy distribution of external resources through the components of the power generation system to be converted and partially destroyed (internal irreversibility) in order to form the final product inherently accompanied by exergetic residuals (external irreversibility). In the case of an ORC, part of the thermal exergy of the residual combustion gases ($\Delta \dot{E}_{g1\text{-}g4}$) is transformed and destroyed in the components of the cycle to generate electrical power. Meanwhile the thermal exergy that is not used from the combustion gases ($\Delta \dot{E}_{g4\text{-}g0}$) is discarded and destroyed in the environment (see Figure 5). Figure 6 shows Grassmann diagrams of the ORC for the refrigerants R134a, R600a, R245fa, and R123 with a condensing temperature of $T_{cond}$ = 25 °C and an exhaust gas temperature at the HRSG outlet of $T_{g4}$ = 100 °C.

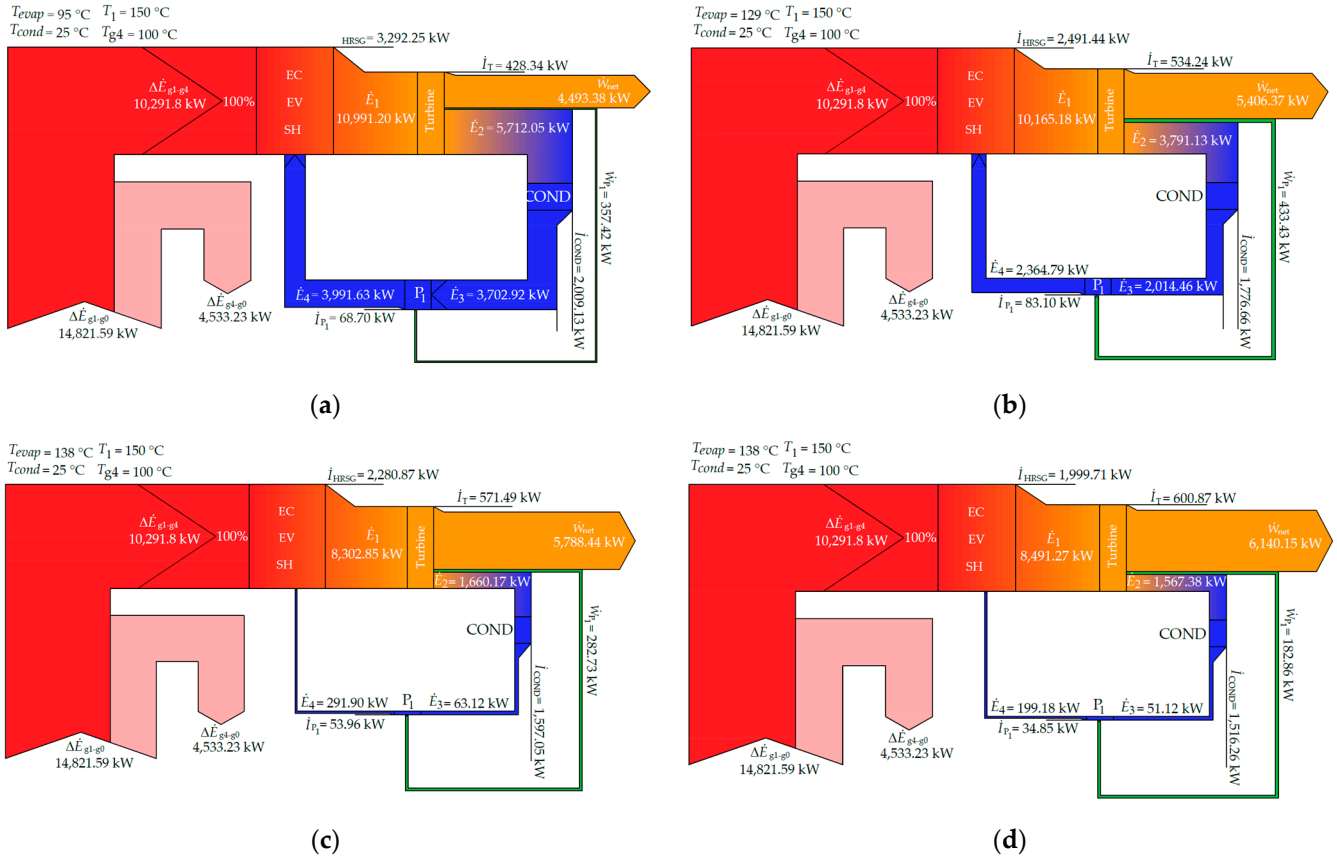


**Figure 6.** Grassmann diagrams of the ORC for the different working fluids: (**a**) R134a, (**b**) R600a, (**c**) R245fa, and (**d**) R123.

For the refrigerants R134a, R245fa, R600a, and R123, the Grassmann diagrams in Figure 6 indicate that only 44, 53, 56, and 60% of the exergy of the residual exhaust gases entering the system was used to generate power, respectively. R134a was the refrigerant

that presented the highest exergy at the turbine inlet $\dot{E}_1$. However, 48% of this exergy was destroyed in the condenser so that the ORC operated with the evaporation and condensation pressure ratio of 5.40 (which was the lowest within the case studies in Figure 6) and produced a power equivalent to 40.88% of $\dot{E}_1$. At the other extreme, the ORC operating with R123 presented the highest pressure ratio, the lowest value of $\dot{E}_1$, and the highest power generation, which corresponded to 72.31% of $\dot{E}_1$.

The exergetic efficiency of a ORC can be calculated as $\eta_{exer} = \dot{W}_{net}/\Delta\dot{E}_{g1\text{-}g4}$, which is expressed in terms of the total irreversibilities of the system results in $\eta_{exer} = 1 - \sum\dot{I}_T/\Delta\dot{E}_{g1\text{-}g4}$ ($T_{g4}$). When there is a decrease in the temperature $T_{g4}$, there will be an increase in the exergy change $\Delta\dot{E}_{g1\text{-}g4}$ and an increase in the flow of irreversibilities, as well as an increase in the exergetic efficiency of the ORC. The behavior of the exergetic efficiency as a function of the temperature of combustion gases at the HRSG outlet is presented in Figure 7. This figure shows that, for the condensation temperatures, the highest exergetic efficiencies of the ORC were obtained when $T_{g4}$ = 100 °C, i.e., the lower the temperature $T_{g4}$, the better the use of the exergetic availability of the exhaust gases. At the same time, the irreversibilities of the EC and T decreased more significantly than the increase in the other components.

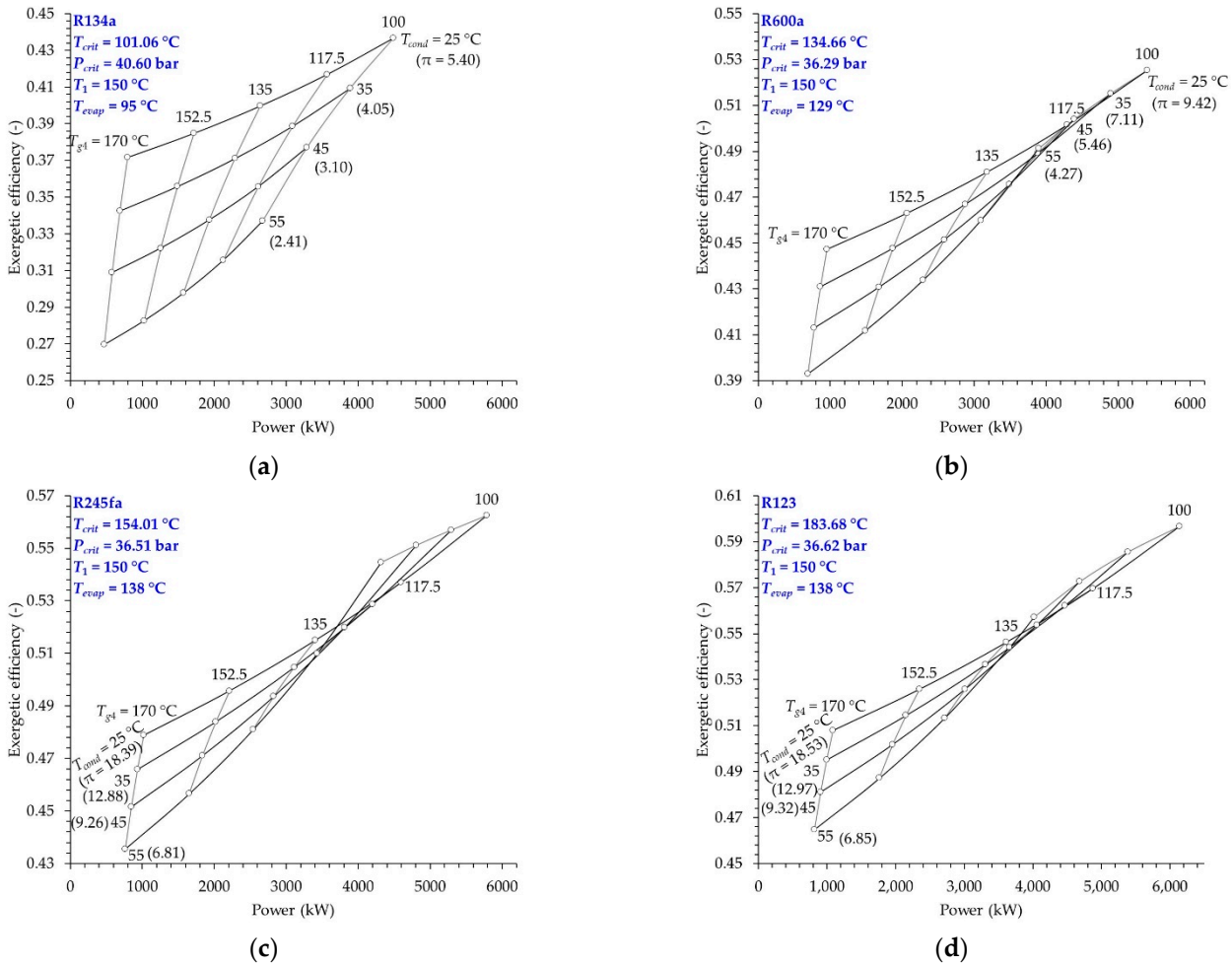


**Figure 7.** Exergetic efficiency and power generated for different condensation temperatures and exhaust gas temperatures at the HRSG outlet: (**a**) R134a, (**b**) R600a, (**c**) R245fa, and (**d**) R123.

The exergetic efficiency decreased as the condensation temperature decreased for a given $T_{g4}$ value between 170 and 100 °C. This was because the cycle power generation decreased with $T_{cond}$.

When comparing the four refrigerants, Figure 7 indicates that the ORC operating with R123 was the system with the highest exergetic efficiencies, followed by R245fa, R600a, and finally R134a.

### *3.4. Evaluation of the Exergy Viability of the Refrigerant in the ORC*

In this section, the refrigerant with the highest exergetic viability index for ranges of condensing temperatures is identified. This was done to select a refrigerant, considering the indices in Table 3, which take into account the power generated by the ORC, the $\Delta T_{PP}$, the unused exergy of residual combustion gases, the *SSC*, the exergetic efficiency of the ORC, the total heat transfer requirement, the global warming potential, and the ozone depletion potential of the refrigerant.

The contributions of the indicators in Table 3 in the exergetic viability indices of the refrigerants for the case studies in Table A2 are presented in Figure 8. From this figure, it can be seen that R134a was the refrigerant with the lowest values from the exergetic viability index. The ORC operating with R245fa, despite not generating the highest amounts of power and being the second refrigerant with the highest total heat transfer requirement, showed the highest exergetic viability index for condensing temperatures of 25, 35, and 45 °C. This was due to the fact that the values of the $\Delta T_{PP}$ ($\alpha_2$) were within the range of 10 to 20 °C, in addition to the presentation of high exergetic efficiencies ($\alpha_5$). Figure 8 indicates that, for a condensing temperature of 45 °C, both R245fa and R600a were viable refrigerants for operation in the ORC. Finally, for condensing temperatures above 45 °C, it was observed that R600a was the most exergetically viable refrigerant used in the ORC because, under these conditions, the $\Delta T_{PP}$ fell in the range of 10 to 20 °C, and it also had a low global warming potential and null ozone depletion potential.

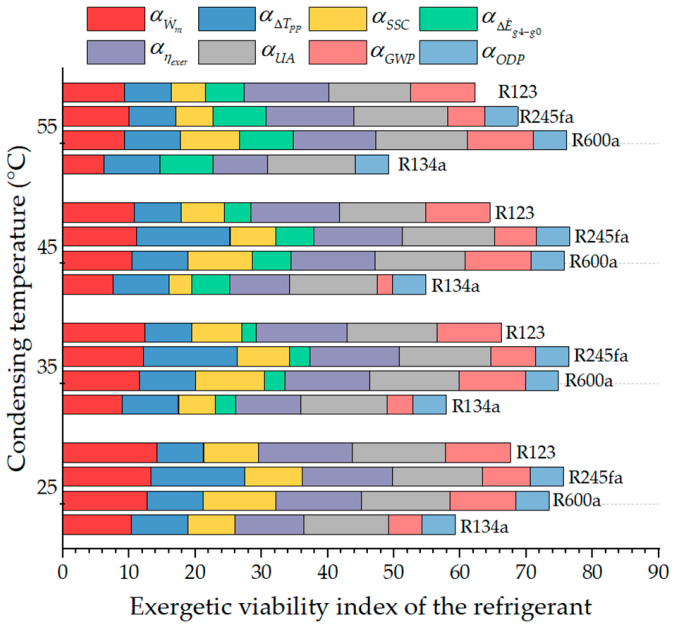


**Figure 8.** Exergetic viability index of the refrigerants in the ORC.

Gyorke et al. [38] proposed a novel classification of pure substances serving as refrigerants based on the entropy sequence of characteristic points on T–s diagrams: primary (A, C, and Z) and secondary points ($M$, $N$, and $M^d$) [39,40]. The primary points A and Z are respectively associated with the lowest (saturated liquid curve side) and highest (saturated vapor curve side) entropies of the saturation curve of the pure substance depicted on the T-s diagram. The primary point C denotes the critical point of the pure substance. If the secondary points $M$, $N$, and $M^d$ exist, they belong to the saturated vapor curve, which can be conceived as a graph of the function $s_g = f(T)$. In this way, the point $N$ is a minimum

of the function $ds_g/dT$ ($T_N$) = 0. The secondary points $M^d$ and $M$ are $S_M{}^d = S_M$ and $T_M{}^d < T_M$. Furthermore, the entropy decreases in the interval [$T_M$, $T_N$), while it increases in the interval ($T_M{}^d$, $T_N$]. In this framework, R134a is an ACZ working fluid, while R600a, R245fa, and R123 are ACNMZ fluids. The results reported by Gyorke et al. [38] indicate that ACNMZ working fluids do not require a superheater if $T_1 < T_{crit}$. This work defined the exergetic viability index to evaluate the feasibility of using a set of working fluids in an ORC system with an HRSG conformed by an EC, an EV, and an SH. However, the methodology presented in this work can be extended to assess different HRSG configurations of ORC systems.

## 4. Conclusions

This work analyzed power generation through an ORC that took advantage of residual combustion gases and studied the use of four refrigerants: R134a, R600a, R245fa, and R123. The study was carried out for four different combinations of evaporation and condensation temperatures with each of the refrigerants. The refrigerant with the highest feasibility of use was determined using the exergetic viability index. This indicator is a weighted average of the absolute deviations with respect to the refrigerant and operating conditions that provide the most favorable amounts for power generation, pinch point temperature difference, unused gas exergy, specific steam consumption, exergetic efficiency, total heat transfer requirement, global warming potential, and ozone depletion potential. Except for the global warming potential and the ozone depletion potential, the other six indicators were quantified from thermodynamic analysis of the ORC for four operating conditions defined by the evaporation and condensation temperatures of the four studied refrigerants. The inclusion of the specific steam consumption, the pinch point temperature difference, and the total heat transfer requirement in the definition of the exergetic viability index was to implicitly consider the size of the equipment, in addition to the power generated by the system. The comparison of the exergetic viability index for the case studies indicated that R245fa and R600a were the most viable refrigerants used in the ORC operation. R245fa was more feasible for use in the ORC at condensing temperatures below 45 °C, while the use of R600a was feasible for condensing temperatures above 45 °C. The proposed indicators and, in general, the thermodynamic analysis methodology could be extended to other refrigerants and different ORC systems.

Furthermore, it is important to add economic indicators to the exergetic viability index in order to give greater certainty to the viability of using a refrigerant in different ORC systems. Therefore, in a future work, an exergoeconomic study will be carried out on different configurations of ORC systems using a new exergetic viability index.

**Author Contributions:** Conceptualization, R.L.-L. and H.L.-M.; methodology, R.L.-L., H.L.-M. and L.E.M.-C.; software, L.E.M.-C.; validation, R.L.-L., H.L.-M. and L.E.M.-C.; formal analysis, R.L.-L., H.L.-M. and L.E.M.-C.; investigation, M.S.-C., M.Á.G.-L. and L.E.M.-C.; resources, R.L.-L. and M.S.-C.; data curation, L.E.M.-C.; writing—original draft preparation, R.L.-L., H.L.-M., T.L.-A. and L.E.M.-C.; writing—review and editing, M.S.-C., M.Á.G.-L., H.L.-M., R.L.-L., T.L.-A. and L.E.M.-C.; visualization, L.E.M.-C.; supervision, M.S.-C. and R.L.-L.; project administration, R.L.-L. All authors have read and agreed to the published version of the manuscript.

**Funding:** This research received no external funding.

**Acknowledgments:** L.E.M.-C. gratefully acknowledges the scholarship from the Mexican National Council for Science and Technology (CONACyT) to pursue his postgraduate studies at UAM-Cuajimalpa.

**Conflicts of Interest:** The authors declare no conflict of interest.

## Nomenclature

**Abbreviations**

| | |
|---|---|
| COND | Condenser |
| HRSG | Heat recovery steam generator |
| EC | Economizer |
| EV | Evaporator |
| ORC | Organic Rankine cycle |
| SH | Superheater |

**Subscripts**

| | |
|---|---|
| 0 | Dead state |
| $1, \ldots, n$ | Thermodynamic states |
| *water* | Cooling water |
| *amb* | Ambient |
| *atm* | Atmospheric |
| *cond* | Condensation |
| *crit* | Critical |
| *evap* | Evaporation |
| *exer* | Exergetic |
| *f* | Saturated liquid |
| *g* | Steam |
| $g1, \ldots, g4$ | Exhaust gases thermodynamic states |
| *g,e* | Exhaust gases |
| *gen* | Generated |
| *HA* | Hot approach |
| *i* | ORC equipment number |
| *in* | Input |
| *IT* | Turbine isentropic efficiency |
| *IP* | Pump isentropic efficiency |
| *j* | ORC thermodynamic state |
| *k* | Working fluid properties |
| *m* | Motor |
| *Make up* | Make-up water |
| *max* | Maximum |
| *out* | Output |
| *p* | Constant pressure |
| *P* | pump |
| *PP* | Pinch point |
| *rej* | Rejected |
| *ref* | Refrigerant |
| *sup* | Supplied |
| *T* | Turbine |
| *th* | Thermal |
| *vc* | Volume control |

**Symbols**

| | | |
|---|---|---|
| $A$ | Area | ($m^2$) |
| $c$ | Specific heat | (kJ/kg °C) |
| $SSC$ | Specific steam consumption | ($kg_{vap}$/kWh) |
| $HR$ | Heat rate | (kJ/kWh) |
| $h$ | Enthalpy per unit mass | (kJ/kg) |
| $\dot{I}$ | Flow of irreversibilities | (kW) |
| $\dot{m}$ | Mass flow | (kg/s) |
| $\dot{Q}$ | Heat flux | (kW) |
| $P$ | Pressure | (bar) |
| $q$ | Heat per unit mass | (kJ/kg) |
| $R$ | Ideal gas constant | (kJ/kg °C) |

| | | |
|---|---|---|
| $s$ | Entropy per unit mass | (kJ/kg °C) |
| $\dot{S}$ | Entropy flow | (kW/°C) |
| $T$ | Temperature | (°C) |
| $UA$ | Total heat transfer requirement | (kW/K) |
| $V$ | Volume | ($m^3$) |
| $w$ | Work per unit mass | (kJ/kg) |
| $\dot{W}$ | Power | (kW) |
| $\dot{W}_L$ | Rate of work lost | (kW) |
| **Greek letters** | | |
| $\Delta$ | Increment | (-) |
| $\dot{E}$ | Exergy flow | (kW) |
| $\varepsilon$ | Specific exergy | (kJ/kg) |
| $\eta$ | Efficiency | (-) |
| $\pi$ | Pressure ratio | (-) |

## Appendix A. Energy Indicators of the ORC Performance for the Different Refrigerants and Exhaust Gas Temperatures at the HRSG Outlet of $T_{g4}$ = 100 °C

**Table A1.** Energetic performance indicators for working fluids.

| Fluid | $T_{evap}$ (°C) | $P_{evap}$ (bar) | $T_{cond}$ (°C) | $P_{cond}$ (bar) | $\pi$ (-) | $w_m$ (kJ/kg$_{ref}$) | $q_{sup}$ (kJ/kg$_{ref}$) | $\eta_{th}$ (-) | $HR$ (kJ/kW h) |
|---|---|---|---|---|---|---|---|---|---|
| R134a | 95 | 35.91 | 25 | 6.65 | 5.40 | 38.10 | 275.83 | 0.138 | 26,061.54 |
| R600a | 129 | 33.02 | | 3.50 | 9.42 | 83.58 | 502.85 | 0.166 | 21,660.48 |
| R245fa | 138 | 27.25 | | 1.48 | 18.39 | 49.28 | 276.94 | 0.178 | 20,230.76 |
| R123 | 138 | 16.93 | | 0.91 | 18.53 | 45.93 | 243.31 | 0.189 | 19,071.92 |
| R134a | 95 | 35.91 | 35 | 8.87 | 4.05 | 31.29 | 261.51 | 0.120 | 30,085.25 |
| R600a | 129 | 33.02 | | 4.65 | 7.11 | 72.01 | 478.27 | 0.151 | 23,910.54 |
| R245fa | 138 | 27.25 | | 2.12 | 12.88 | 42.90 | 263.60 | 0.163 | 22,118.66 |
| R123 | 138 | 16.93 | | 1.31 | 12.97 | 40.32 | 233.05 | 0.173 | 20,806.07 |
| R134a | 95 | 35.91 | 45 | 11.60 | 3.10 | 24.94 | 246.77 | 0.101 | 35,616.83 |
| R600a | 129 | 33.02 | | 6.04 | 5.46 | 61.22 | 453.03 | 0.135 | 26,640.10 |
| R245fa | 138 | 27.25 | | 2.94 | 9.26 | 36.94 | 250.04 | 0.148 | 24,364.94 |
| R123 | 138 | 16.93 | | 1.82 | 9.32 | 35.05 | 222.67 | 0.157 | 22,873.28 |
| R134a | 95 | 35.91 | 55 | 14.92 | 2.41 | 19.04 | 231.51 | 0.082 | 43,767.09 |
| R600a | 129 | 33.02 | | 7.73 | 4.27 | 51.19 | 427.09 | 0.120 | 30,037.15 |
| R245fa | 138 | 27.25 | | 4.00 | 6.81 | 31.39 | 236.23 | 0.133 | 27,094.12 |
| R123 | 138 | 16.93 | | 2.47 | 6.85 | 30.08 | 212.16 | 0.142 | 25,390.76 |

**Table A2.** Variation of power and other parameters for the working fluids.

| Fluid | $T_{g4}$ (°C) | $T_{cond}$ (°C) | $\dot{m}_{ref}$ (kg$_{ref}$/s) | $\dot{W}_m$ (kW) | $\Delta T_{PP}$ (°C) | $\dot{Q}_{sup}$ (kW) | $\dot{Q}_{rej}$ (kW) | $\dot{m}_{water}$ (kg$_{water}$/s) | $SSC$ (kg$_{ref}$/kW h) | $GWP$ | $ODP$ |
|---|---|---|---|---|---|---|---|---|---|---|---|
| R134a | 100 | 25 | 117.89 | 4491.87 | 41.26 | 32,518.08 | 28,026.21 | 629.74 | 94.48 | 1430 | 0 |
| | | 35 | 124.35 | 3891.11 | 38.59 | | 28,626.97 | 684.61 | 115.04 | | |
| | | 45 | 131.78 | 3286.79 | 35.52 | | 29,231.29 | 699.42 | 144.33 | | |
| | | 55 | 140.46 | 2674.73 | 31.93 | | 29,843.36 | 713.92 | 189.05 | | |
| R600a | 100 | 25 | 64.67 | 5404.55 | 23.44 | 32,518.08 | 27,113.54 | 647.28 | 43.07 | 5 | 0 |
| | | 35 | 67.99 | 4895.96 | 21.77 | | 27,622.12 | 660.58 | 49.99 | | |
| | | 45 | 71.78 | 4394.32 | 19.86 | | 28,123.77 | 672.92 | 58.80 | | |
| | | 55 | 76.14 | 3897.34 | 17.67 | | 28,620.74 | 684.67 | 70.33 | | |

**Table A2.** *Cont.*

| Fluid | $T_{g4}$ (°C) | $T_{cond}$ (°C) | $\dot{m}_{ref}$ ($kg_{ref}/s$) | $\dot{W}_m$ (kW) | $\Delta T_{PP}$ (°C) | $\dot{Q}_{sup}$ (kW) | $\dot{Q}_{rej}$ (kW) | $\dot{m}_{water}$ ($kg_{water}/s$) | SSC ($kg_{ref}$/kW h) | GWP | ODP |
|---|---|---|---|---|---|---|---|---|---|---|---|
| R245fa | 100 | 25 | 117.42 | 5786.49 | 14.44 | 32,518.08 | 26,731.59 | 638.16 | 73.05 | 1030 | 0 |
| | | 35 | 123.36 | 5292.59 | 12.79 | | 27,225.49 | 651.09 | 83.91 | | |
| | | 45 | 130.05 | 4804.65 | 10.94 | | 27,713.43 | 663.10 | 97.45 | | |
| | | 55 | 137.65 | 4320.68 | 8.83 | | 28,197.40 | 674.54 | 114.69 | | |
| R123 | 100 | 25 | 133.64 | 6137.84 | 5.62 | 32,516.75 | 26,378.92 | 629.74 | 78.39 | 77 | 0.02 |
| | 103.59 | 35 | 133.64 | 5388.99 | | 31,145.50 | 25,756.50 | 615.96 | 89.28 | | |
| | 107.21 | 45 | 133.64 | 4683.62 | | 29,758.29 | 25,074.66 | 599.96 | 102.72 | | |
| | 110.88 | 55 | 133.64 | 4020.22 | | 28,354.56 | 24,334.34 | 582.13 | 119.67 | | |

## Appendix B. Exergy Indicators of the ORC Performance for Different Refrigerants and Exhaust Gas Temperatures at the HRSG Outlet for $T_{g4}$ = 100 °C

**Table A3.** Flow of irreversibility, exergy flow of exhaust gas, and exergetic efficiency.

| Fluid | $T_{cond}$ (°C) | $\dot{I}_T$ (kW) | $\dot{I}_B$ (kW) | $\dot{I}_{HRSG}$ (kW) | $\dot{I}_{COND}$ (kW) | $\dot{I}_{TOTAL}$ (kW) | $\dot{E}_{g,e}$ (kW) | $\eta_{exer}$ (-) |
|---|---|---|---|---|---|---|---|---|
| R134a | 25 | 428.34 | 68.71 | 3292.26 | 2009.14 | 5798.44 | 10,291.83 | 0.44 |
| R600a | | 534.24 | 83.11 | 2491.44 | 1776.67 | 4885.45 | | 0.53 |
| R245fa | | 571.50 | 53.96 | 2280.87 | 1597.05 | 4503.38 | | 0.56 |
| R123 | | 600.87 | 34.80 | 1999.72 | 1516.27 | 4151.67 | | 0.60 |
| R134a | 35 | 378.26 | 69.53 | 3144.91 | 2021.36 | 5614.06 | 9506.48 | 0.41 |
| R600a | | 495.00 | 86.31 | 2289.46 | 1738.09 | 4608.86 | | 0.52 |
| R245fa | | 531.60 | 56.62 | 2060.68 | 1563.20 | 4212.09 | | 0.56 |
| R123 | | 533.59 | 34.64 | 1819.94 | 1428.03 | 3816.20 | 9207.23 | 0.59 |
| R134a | 45 | 326.56 | 69.06 | 3000.30 | 2037.31 | 5433.23 | 8721.13 | 0.38 |
| R600a | | 455.24 | 89.20 | 2083.40 | 1697.49 | 4325.32 | | 0.50 |
| R245fa | | 491.51 | 59.18 | 1836.95 | 1527.21 | 3914.85 | | 0.55 |
| R123 | | 469.62 | 34.21 | 1653.59 | 1339.26 | 3496.68 | 8182.07 | 0.57 |
| R134a | 55 | 272.46 | 66.66 | 2860.87 | 2060.16 | 5260.15 | 7935.78 | 0.34 |
| R600a | | 414.55 | 91.55 | 1874.92 | 1656.10 | 4037.11 | | 0.49 |
| R245fa | | 450.86 | 61.52 | 1611.24 | 1490.01 | 3613.63 | | 0.54 |
| R123 | | 408.66 | 33.44 | 1501.58 | 1250.87 | 3194.55 | 7216.29 | 0.56 |

## References


1. Mahmoudi, A.; Fazli, M.; Morad, M.R. A recent review of waste heat recovery by Organic Rankine Cycle. *Appl. Therm. Eng.* **2018**, *143*, 660–675. [CrossRef]
2. Zare, V. A comparative exergoeconomic analysis of different ORC configurations for binary geothermal power plants. *Energy Convers. Manag.* **2015**, *105*, 127–138. [CrossRef]
3. Blondel, Q.; Tauveron, N.; Caney, N.; Voeltzel, N. Experimental study and optimization of the Organic Rankine Cycle with pure NovecTM649 and zeotropic mixture NovecTM649/HFE7000 as working fluid. *Appl. Sci.* **2019**, *9*, 1865. [CrossRef]
4. SGarcia, I.; Garcia, R.F.; Carril, J.C.; Garcia, D.I. A review of thermodynamic cycles used in low temperature recovery systems over the last two years. *Renew. Sustain. Energy Rev.* **2018**, *81*, 760–767. [CrossRef]
5. Salazar-Pereyra, M.; Mora-Ortega, A.; Bonilla-Blancas, A.E.; Lugo-Leyte, R.; Lugo-Méndez, H.D. Parametric analysis of the geothermal power: Dry-steam, flash steam and hybrid cycle. *DYNA* **2017**, *84*, 273–282. [CrossRef]
6. Dai, B.; Zhu, K.; Wang, Y.; Sun, Z.; Liu, Z. Evaluation of organic Rankine cycle by using hydrocarbons as working fluids: Advanced exergy and advanced exergoeconomic analyses. *Energy Convers. Manag.* **2019**, *197*, 111876. [CrossRef]
7. Fan, W.; Han, Z.; Li, P.; Jia, Y. Analysis of the thermodynamic performance of the organic Rankine cycle (ORC) based on the characteristic parameters of the working fluid and criterion for working fluid selection. *Energy Convers. Manag.* **2020**, *211*, 112746. [CrossRef]
8. Vélez, F. Selecting working fluids in an organic Rankine cycle for power generation from low temperature heat sources. *Dyna* **2014**, *81*, 173–180. [CrossRef]

9. Gonzalez-Contreras, M.; Lugo-Mendez, H.; Sales-Cruz, M.; Lopez-Arenas, T. Synthesis, design and evaluation of intensified lignocellulosic biorefineries-Case study: Ethanol production. *Chem. Eng. Process. Process Intensif.* **2021**, *159*, 108220. [CrossRef]
10. Jankowski, M.; Borsukiewicz, A. A novel exergy indicator for maximizing energy utilization in low-temperature ORC. *Energies* **2020**, *13*, 1598. [CrossRef]
11. Kolasinski, P. The method of the working fluid selection for organic Rankine cycle (ORC) systems employing volumetric expanders. *Energies* **2020**, *13*, 573. [CrossRef]
12. Kajurek, J.; Rusowicz, A.; Grzebielec, A.; Bujalski, W.; Futyma, K.; Rudowicz, Z. Selection of refrigerants for a modified organic Rankine cycle. *Energy* **2019**, *168*, 1–8. [CrossRef]
13. Raghulnath, D.; Saravanan, K.; Mahendran, J.; Kumar, M.R.; Lakshmanan, P. Analysis and optimization of organic Rankine cycle for IC engine waste heat recovery system. *Mater. Today Proc.* **2020**, *21*, 30–35. [CrossRef]
14. Mohamed, H.; Bani-Hani, E.; Assad, M.E.H. Thermal Analysis of Organic Rankine Cycle Using Different Organic Fluids. *Renew. Energy Res. Appl.* **2020**, *1*, 115–121. [CrossRef]
15. Vélez, F.; Chejne, F.; Quijano, A. Thermodynamic analysis of R134a in an Organic Rankine Cycle for power generation from low temperature sources. *Dyna* **2014**, *81*, 153. [CrossRef]
16. Wang, J.; Yan, Z.; Wang, M.; Ma, S.; Dai, Y. Thermodynamic analysis and optimization of an (organic Rankine cycle) ORC using low grade heat source. *Energy* **2013**, *49*, 356–365. [CrossRef]
17. Abadi, G.B.; Yun, E.; Kim, K.C. Experimental study of a 1 kw organic Rankine cycle with a zeotropic mixture of R245fa/R134a. *Energy* **2015**, *93*, 2363–2373. [CrossRef]
18. Surindra, M.D.; Caesarendra, W.; Prasetyo, T.; Mahlia, T.M.I. Taufik Comparison of the utilization of 110 °C and 120 °C heat sources in a geothermal energy system using Organic Rankine Cycle (ORC) with R245fa, R123, and mixed-ratio fluids as working fluids. *Processes* **2019**, *7*, 113. [CrossRef]
19. Nondy, J.; Gogoi, T.K. Comparative performance analysis of four different combined power and cooling systems inte-grated with a topping gas turbine plant. *Energy Convers. Manag.* **2020**, *223*, 113242. [CrossRef]
20. Jannatkhah, J.; Najafi, B.; Ghaebi, H. Energy and exergy analysis of combined ORC–ERC system for biodiesel-fed diesel engine waste heat recovery. *Energy Convers. Manag.* **2020**, *209*, 112658. [CrossRef]
21. Liao, G.; Jiaqiang, E.; Zhang, F.; Chen, J.; Leng, E. Advanced exergy analysis for Organic Rankine Cycle-based layout to recover waste heat of flue gas. *Appl. Energy* **2020**, *266*, 114891. [CrossRef]
22. Boyaghchi, F.A.; Montazerinejad, H. Multi-objective optimisation of a novel combined cooling, heating and power system integrated with flat plate solar collectors using water/CuO nanofluid. *Int. J. Exergy* **2016**, *21*, 202–238. [CrossRef]
23. Tiwari, D.; Sherwani, A.F.; Atheaya, D.; Kumar, A.; Kumar, N. Thermodynamic analysis of Organic Rankine cycle driven by reversed absorber hybrid photovoltaic thermal compound parabolic concentrator system. *Renew. Energy* **2020**, *147*, 2118–2127. [CrossRef]
24. Tontu, M.; Sahin, B.; Bilgili, M. An exergoeconomic–environmental analysis of an organic Rankine cycle system integrated with a 660 MW steam power plant in terms of waste heat power generation. *Energy Sources Part A Recover. Util. Environ. Eff.* **2020**, 1–22. [CrossRef]
25. Gao, H.; Liu, C.; He, C.; Xu, X.; Wu, S.; Li, Y. Performance analysis and working fluid selection of a supercritical organic rankine cycle for low grade waste heat recovery. *Energies* **2012**, *5*, 3233–3247. [CrossRef]
26. Liu, G.; Wang, Q.; Xu, J.; Miao, Z. Exergy analysis of two-stage organic rankine cycle power generation system. *Entropy* **2021**, *23*, 43. [CrossRef]
27. Baral, S.; Kim, D.; Yun, E.; Kim, K.C. Experimental and thermoeconomic analysis of small-scale solar organic rankine cycle (SORC) system. *Entropy* **2015**, *17*, 2039–2061. [CrossRef]
28. Zhang, X.; Cao, M.; Yang, X.; Guo, H.; Wang, J. Economic analysis of Organic Rankine Cycle using R123 and R245fa as working fluids and a demonstration project report. *Appl. Sci.* **2019**, *9*, 288. [CrossRef]
29. Restrepo, G.; Weckert, M.; Brüggemann, R.; Gerstmann, S.; Frank, H. Ranking of refrigerants. *Environ. Sci. Technol.* **2008**, *42*, 2925–2930. [CrossRef]
30. Lemmon, E.; Huber, M.; McLinden, M. *"NIST Standard Reference Database 23: Reference Fluid Thermodynamic and Transport Properties-REFPROP, Version 9.1." In Natl Std. Ref. Data Series (NIST NSRDS)*; National Institute of Standards and Technology: Gaithersburg, MD, USA, 2013. Available online: https://tsapps.nist.gov/publication/get_pdf.cfm?pub_id=912382 (accessed on 15 January 2022).
31. Guo, T.; Wang, H.; Zhang, S. Comparative analysis of CO2-based transcritical Rankine cycle and HFC245fa-based subcritical organic Rankine cycle using low-temperature geothermal source. *Sci. China Technol. Sci.* **2010**, *53*, 1638–1646. [CrossRef]
32. He, C.; Liu, C.; Gao, H.; Xie, H.; Li, Y.; Wu, S.; Xu, J. The optimal evaporation temperature and working fluids for subcritical organic Rankine cycle. *Energy* **2012**, *38*, 136–143. [CrossRef]
33. Karellas, S.; Schuster, A.; Leontaritis, A.D. Influence of supercritical ORC parameters on plate heat exchanger design. *Appl. Therm. Eng.* **2012**, *33–34*, 70–76. [CrossRef]
34. El-Sattar, H.A.; Kamel, S.; Vera, D.; Jurado, F. Tri-generation biomass system based on externally fired gas turbine, organic rankine cycle and absorption chiller. *J. Clean. Prod.* **2020**, *260*, 121068. [CrossRef]
35. Karellas, S.; Braimakis, K. Energy-exergy analysis and economic investigation of a cogeneration and trigeneration ORC-VCC hybrid system utilizing biomass fuel and solar power. *Energy Convers. Manag.* **2016**, *107*, 103–113. [CrossRef]

36. Zhi, L.H.; Hu, P.; Chen, L.X.; Zhao, G. Thermodynamic analysis of a novel transcritical-subcritical parallel organic Rankine cycle system for engine waste heat recovery. *Energy Convers. Manag.* **2019**, *197*, 111855. [CrossRef]
37. COko, O.C.; Njoku, I.H. Performance analysis of an integrated gas-, steam-and organic fluid-cycle thermal power plant. *Energy* **2017**, *122*, 431–443. [CrossRef]
38. Matuszewska, D.; Olczak, P. Evaluation of using gas turbine to increase efficiency of the organic Rankine cycle (ORC). *Energies* **2020**, *13*, 1499. [CrossRef]
39. Györke, G.; Deiters, U.K.; Groniewsky, A.; Lassu, I.; Imre, A.R. Novel classification of pure working fluids for Organic Rankine Cycle. *Energy* **2018**, *145*, 288–300. [CrossRef]
40. Imre, A.R.; Kustán, R.; Groniewsky, A. Mapping of the temperature-entropy diagrams of van der Waals fluids. *Energies* **2020**, *13*, 1519. [CrossRef]